THIRTEENTH EUROPEAN ROTORCRAFT FORUM

1-2

Paper No. 16

COMPUTATION OF NON-LINEAR ACOUSTICS IN TWO-DIMENSIONAL BLADE-VORTEX INTERACTIONS

J. D. BAEDER

U.S. ARMY AEROFLIGHTDYNAMICS DIRECTORATE

NASA AMES RESEARCH CENTER

MOFFETT FIELD, CA USA

September 8-11, 1987

ARLES, FRANCE

ASSOCIATION AERONAUTIQUE ET ASTRONAUTIQUE DE FRANCE

COMPUTATION OF NON-LINEAR ACOUSTICS IN TWO-DIMENSIONAL BLADE-VORTEX INTERACTIONS

J. D. Baeder

U.S. Army Aeroflightdynamics Directorate - AVSCOM
NASA Ames Research Center
Moffett Field, California 94035 USA

1. Abstract

The propagation characteristics of the interaction between a vortex and a helicopter airfoil have been investigated over a wide variety of methods, ranging from Linearized Transonic Small Disturbance to Thin-layer Navier-Stokes. The effect of numerical algorithms and methods on the acoustics has been clearly demonstrated. In addition, the Euler equations were utilized to study the effect of transonic flow on the formation process of the acoustic wave, resulting in significant new insight. The effect of the interaction distance was studied by looking at the cases of a vortex passing below the airfoil, the vortex having a head-on collision with the airfoil, and a vortex passing above the airfoil. For supercritical flows the resulting acoustic wave is much larger for an observer below the airfoil when the vortex passes above the airfoil rather than below it. This suggests that one should avoid situations which result in the vortex passing above the airfoil.

2. Notation

c	=	chord length
C_2	=	$-\frac{1}{2}(\gamma+1)M_\infty^2$
C_3	=	$-(\gamma-1)M_\infty^2$
C_p	=	coefficient of pressure
C_{p_i}	=	initial coefficient of pressure
e	=	total energy per unit volume
J	=	Jacobian of transformation
M_∞	=	free stream Mach number
p	=	static pressure
Re	=	Reynolds number
R	=	nondimensional distance to source in acoustic frame
u, v	=	nondimensional velocities
U, V	=	contravariant velocity components
u_v, v_v	=	nondimensional velocities induced by the vortex
x, y, τ, ξ, η	=	nondimensional coordinates
x_v, y_v	=	nondimensional vortex location
β^2	=	$1 - M_\infty^2$
Γ_v	=	nondimensional vortex strength
ρ	=	density
ϕ	=	velocity potential

3. Introduction

The transonic flow phenomena that occur on the advancing blade tips of modern helicopters have major effects on the aerodynamic performance, vibratory loads, and acoustic

radiation of the rotor. One of the primary influences on the advancing blade is the blade-vortex interaction which can result in large variations in the lift, moment, and drag with a corresponding propagation of acoustic energy to the far-field.

A variety of computational procedures for calculating the unsteady interaction of a helicopter rotor blade with a Lamb-like vortex of finite viscous core in subsonic and transonic flows have been developed for the limiting case of a two-dimensional parallel blade-vortex interaction [1-5] as shown in Figure 1. In all of these studies, the method and grid was chosen to enhance the accuracy of the airloads by clustering points near the airfoil, while neglecting the acoustics. In addition, several studies have been performed to examine the resulting acoustics [1,6-8]. However, in most of these studies either the grid resolution was inadequate [1], incompressible methods were used [6], or linear methods of propagating the waves were used in regions that might still have non-linear effects [7]. As shown in [8], one must be very careful in using traditional Computational Fluid Dynamic (CFD) methods to calculate acoustic waves.

In [8] it was shown that acoustic waves can be properly captured when careful attention is paid to the grid resolution. However, it was uncertain what the effects of the small-disturbance assumptions had on the initial development of the acoustic wave and the non-linear wave steepening and acoustic propagation from the near field. Also, newer high-order upwind-biased numerical schemes have been developed recently [5] to increase the accuracy of calculations. Therefore, it is necessary to compare the acoustic propagations as determined by a wide spectrum of methodologies and algorithms. In addition, one must use a non-perturbation approach [5] to examine the acoustic propagation resulting from a head-on collision.

4. Considerations for Acoustic CFD

In order to properly capture the acoustics of the blade-vortex interaction one must first have an accurate calculation of the aerodynamics on the airfoil surface. In the subcritical regime, the pressure fluctuations are primarily concentrated in the leading edge region and therefore one must accurately calculate the flow in that region.

In the supercritical regime, the changes in the flowfield are no longer confined to the leading edge region. As seen in Figure 2, there may be large fluctuations in the middle of the airfoil due to the movement of the shocks as the vortex passes by. Another factor complicating the acoustics is the fact that supersonic regions are formed, which inhibit the transfer of disturbances upstream. Thus, it also becomes important aerodynamically to accurately calculate the point where the transition to supersonic flow takes place. Often this sonic line is just downstream from the leading edge. If this region is not accurately calculated it could have a dramatic influence on the manner in which the acoustics is propagated.

The variation in pressure on the airfoil due to the vortex interaction is at least an order of magnitude greater than that off of the airfoil. Thus, the correct calculation of the acoustics requires a method that not only accurately calculates the aerodynamics on the airfoil, but one that will also properly preserve and propagate the wave as it leaves the surface. This will require a grid that can maintain the acoustics wave structure and also a numerical method that has high accuracy and a minimum of dissipation, otherwise the acoustic wave will be quickly distorted and dissipated.

Just as important as the accurate calculation of the acoustic information is the method of analyzing the data, otherwise useful information might be missed and incorrect conclusions might be drawn. It is important to be able to separate the acoustics from the near-field aerodynamics and to scale the acoustical data. In order to do this one must first of all realize that the flow is being perturbed around the steady-state solution, thus it is logical to subtract

out the initial steady-state solution without the vortex. Secondly, the primary disturbance occurs when the vortex passes by the leading edge and thus it is logical to think of the problem as occuring in a frame of reference where the observer is fixed in space relative to the acoustic source with the airfoil moving past at freestream Mach number. This is illustrated by Figure 3 which shows this observer fixed in space frame of reference and compares it to a frame of reference in which the observer is fixed with respect to the airfoil. This approximates a rotor blade passing over a ground based observer in the limiting case of the advance ratio approaching zero. Thirdly, in two-dimensional acoustics the amplitude falls off as the square-root of the distance to the source. As a result the acoustics is best analyzed by looking at quantities perturbed from the steady-state and scaled by the square-root of the distance to the vortex. This was previously shown by the author [8]. In this paper, contour plots of the scaled pressure disturbance will be displayed in color. Red lines represent negative scaled pressure disturbance values, while blue lines represents positive scaled pressure disturbance values. Thus, the transition from red to blue represents a compression wave and the transition from blue to red represents an expansion wave. Time histories of the scaled pressure disturbance at selected points in the flowfield will also be shown (Figure 4).

5. Description of Methods Used

The first two methods to be examined are the Linearized Small Disturbance Equation (LTSD) and the Transonic Small Disturbance Equation (TSD). These were both studied by using the code ATRAN2 [9-10]. The effects of the vortex are included by using a perturbation technique [3]. The boundary condition was changed to include the effect of the vortex on the streamwise component of velocity. Also, higher order non-linear terms were included in the y-direction in order to better approximate the propagation of the waves. Hence, the Transonic Small Disturbance Equation solved is as follows

$$M_\infty^2 \phi_{tt} + 2M_\infty^2 \phi_{xt} =$$

$$\frac{\partial}{\partial x}[(\beta^2 + C_2\phi_x + C_3\phi_t)(\phi_x + u_v) - \beta^2 u_v] + [1 + C_3(\phi_x + \phi_t)]\phi_{yy}$$

with the boundary condition on the airfoil

$$\phi_y(x, y \to 0) = (1 + u_v)y_x + y_t - v_v$$

The Linear Small Disturbance Equation was solved by setting the non-linear terms above to zero. The ATRAN2 algorithm is implicit and it is first-order accurate in space and time. No explicit dissipation is added. The mesh is cartesian and since the method is only first-order accurate in space a fairly fine grid is required in the region in front of and on the airfoil. For the calculations in this paper a 399x195 mesh was used, resulting in a CPU time on the order of ten minutes on a CRAY-XMP for thirty chords of travel.

The second two methods to be examined are the Euler and Navier-Stokes Equations. These are as follows

$$\frac{\partial \widehat{Q}}{\partial \tau} + \frac{\partial \widehat{E}}{\partial \xi} + \frac{\partial \widehat{F}}{\partial \eta} = \epsilon \frac{1}{Re} \frac{\partial \widehat{S}}{\partial \eta}$$

where

$$\widehat{Q} = J^{-1}\begin{bmatrix}\rho\\ \rho u\\ \rho v\\ e\end{bmatrix},\ \widehat{E} = J^{-1}\begin{bmatrix}\rho U\\ \rho u U + \xi_x p\\ \rho v U + \xi_y p\\ U(e+p) - \xi_t p\end{bmatrix},\ etc.$$

and

$\epsilon = 0 \rightarrow$ Euler Equations

$\epsilon = 1 \rightarrow$ Thin Layer Navier-Stokes Equations

The Euler equations were studied by setting the viscous terms to zero and imposing tangency at the body instead of the no-slip boundary condition. These equations were then solved using the zonal code of [5]. The algorithm in this case is upwind-biased, and fifth-order accurate in space and second-order accurate in time. Since it is upwind-biased there is no explicit artificial dissipation added to stabilize the algorithm. For the vortex interactions the flowfield is divided into three zones as shown in Figure 5. Each zone contains from 13,000 to 20,000 grid points. Note that a fine grid is placed upstream of the airfoil. This, combined with the high-order accuracy of the algorithm allows for the vortex to be captured without a perturbation scheme. Thus, the vortex is placed in the flowfield and convects with the local velocity and is allowed to deform as it approaches the airfoil. The CPU time for the Euler calculations were on the order of four hours on a CRAY-XMP for twenty chords of travel.

6. Comparison of Results

It was decided to test the various methods for the same case of a vortex of non-dimensional strength of 0.2 passing 0.26 chords underneath a NACA 0012 airfoil at a Mach number of 0.8. The resulting solutions will help aid in evaluating the usefulness of the different methods in calculating the acoustics of blade-vortex interactions in the transonic regime. Contour plots of the scaled pressure disturbance with the vortex 8 chords downstream are shown in Figure 6 for the four different methods. The straight white lines indicate distances of five chords above, below, behind, and in front of the leading edge. The boundaries of the small disturbance calculations extend several hundred chords away and only a limited portion of the flowfield is shown. However, the boundaries for the Euler and Navier-Stokes calculations are quite near and thus the complete flowfields are shown. In addition, time histories of the scaled pressure disturbance are displayed for several locations in Figure 7.

The contour plots show that the LTSD solution is very anti-symmetric about the y=0 line. In other words, although the wave shapes are exactly the same, the amplitudes are of opposite sign above and below the airfoil. Since the non-linear terms are neglected, the acoustic wave propagates at a constant speed and the waves above and below the airfoil are at the same distance in front of the airfoil. The time history plots verify that the acoustic wave is smooth and well preserved, with the wave above the airfoil being almost exactly the opposite of that below the airfoil. In addition, the amplitude of the disturbance on axis is very small and seems to increase until one reaches an angle of approximately 40 degrees.

The TSD solution is not as anti-symmetric as the LTSD solution. Since shock waves form on both surfaces the field is highly non-linear in the vicinity of the airfoil. This results in supersonic pockets where the acoustic propagation in the upstream direction is inhibited and delayed. Thus, the wave is split into two parts in the upstream direction. The portion of the disturbance on the airfoil that takes place before the flow becomes supersonic is able to propagate forward, while that which takes place in the region of the airfoil which is supersonic is forced to propagate downstream until it leaves the supersonic pocket. This can be seen in the contour plot, where the propagation above the airfoil seems to be split into two waves and

the propagation below the airfoil seems to primarily consist of a wave that has been delayed by the supersonic region. Also, the amplitude of the propagated wave seems to be much larger above the airfoil than below the airfoil. These ideas are confirmed in the time history plots.

The Euler and Navier-Stokes solutions are nearly identical. From this it would appear that viscous effects are unimportant for this particular case where large-scale separation does not occur. The acoustic wave is fairly anti-symmetric. However, unlike the TSD solution, these both appear to have a strong wave both above and below the airfoil. One can also see that the fifth-order upwind-biased algorithm does a very good job at capturing and maintaining the sharp structures of the acoustic wave. Near the axis the wave is seen to be broken into two parts with a flat section in between. This would appear to be due to the supersonic pockets on the upper and lower surfaces. As was the case using the LTSD and TSD, it appears that the amplitude of the wave is greater above the airfoil than below it.

Overall, all four methods agree very well for the portion of the acoustic wave above the airfoil. The time history plots at 30 degrees above the airfoil are all very similar. It would seem that at this position the non-linear effects are small and both the LTSD and TSD equations are adequate. The agreement is not quite as good for the points 45 degrees below the airfoil. Although non-linear effects seem to be small in this region (the LTSD solution calculates peak pressures nearly identical to those from the Euler and Navier-Stokes calculations) it appears that there is some deficiency in the TSD Equation formulation, resulting in peak pressure amplitudes that are greatly reduced. Closer to on axis there is even more of a discrepancy. The TSD solution seems to underpredict the first portion of the wave and overpredict the second part. This could also be due to an improper calculation of the transition from subsonic to supersonic flow in the vicinity of the leading edge, where the small disturbance assumption breaks down. Since non-linear effects are important closer to on axis, the LTSD solution no longer predicts the correct peak pressure amplitude. All four methods seem to indicate that non-linear efects decay to unimportant levels once the wave has traveled six chords away form the vortex. The LTSD and TSD methods seem to be unsuitable for detailed comparisons below the airfoil, due to the inaccurate formation of the acoustic waves.

7. Formation of Acoustic Waves In Supercritical Flows

The Euler Equations were utilized to investigate the initial formation of the acoustic wave in supercritical flow by examining in detail the same case as above, but at earlier times. Figure 8 displays a close-up view of the scaled pressure disturbance contours when the vortex is near the airfoil. The white lines in Figure 8a represent the zonal boundaries and it can be seen that the contours are smooth across the zonal boundaries. These lines are not shown in the rest of the Figure. The approximate vortex location is shown by the circular arrow. In addition, the sonic line (where the local Mach number is unity) is shown by the black line.

In the first frame (Figure 8a), the vortex has just passed the leading edge of the airfoil. The sonic point on the lower surface has moved forward to just behind the leading edge, while on the upper surface the sonic point is farther aft. Consequently, the disturbance in the leading edge region appears to be propagating forward primarily on the upper surface. As the vortex travels downstream, most of the disturbance on the lower surface seems to propagate downstream until it reaches the shock (Figure 8c). Part of the disturbance is able to leave the supersonic pocket near the outer region of the shock (Figure 8d,e). However, the rest of the disturbance seems to build up at the foot of the shock. This combines with the disturbance at the shock due to the vortex passage. This disturbance, along with the disturbance from the trailing edge region, does not leave the vicinity of the airfoil until a much later time due to the presence of the supersonic pocket (Figure 6c).

8. Subcritical Cases Using a Zonal Euler Algorithm

It was decided from the above investigation that the TSD seemed to be inadequate in accurately capturing the acoustic wave, while the Navier-Stokes equations are not necessary for unseparated or only moderately separated flows. Thus, three purely subcritical cases (NACA0012 at Mach .6) were investigated using the Euler equations. The three cases to be compared are a vortex interaction that passes below the airfoil, a head-on collision, and a vortex interaction that passes above the airfoil. Contour plots of the scaled pressure disturbance with the vortex 5 chords downstream are shown in Figure 9 for these three cases. The time history plots are displayed in Figure 10.

It is interesting to note that for the cases of the vortex passing above and below the airfoil the shape of the resulting acoustic waves appear to be mirror images. The head-on collision results in an acoustic pattern that is anti-symmetrical. The waves are fairly smooth and the non-linearities are small enough that there does not seem to be appreciable flattening of the expansion waves or steepening of the compression waves. Furthermore, the variation in propagation speed seems to be very small. In all three cases, there is also a second disturbance related to the passage of the vortex near the trailing edge. As expected this, as well as the disturbance related to the passage of the vortex near the leading edge, is more pronounced in the case of the head-on collision. Overall, the effects of the miss distance appear to be very small in the subcritical cases.

9. Supercritical Cases Using a Zonal Euler Algorithm

Three supercritical cases (NACA0012 at Mach .8) were also investigated using the Euler Equations. This should help in understanding better the effect of non-linearities on the solution. The first case, vortex passing below the airfoil, is the same as that performed in the comparison of the four methods. The second and third cases are the passage of the vortex above the airfoil and a head-on collision. Contour plots of the scaled pressure disturbance with the vortex 10 chords downstream are shown in Figure 11 for these three cases. The time history plots are displayed in Figure 12.

As was noted for the subcritical cases it appears that the cases of the vortex passing above and below the airfoil result in acoustic waves that are nearly mirror images of each other. However, for these supercritical cases the variation in wave speed is much larger and the expansion waves tend to flatten while the compression waves steepen. Note also that the head-on case is not as anti-symmetric as it was when the flow was subcritical. It is also apparent that the supersonic regions have caused a delay in the propagation of part of the disturbance, resulting in a relatively flat region near the axis of the airfoil. In the time history plots this results in the wave being separated into two parts. The time histories also show that the position of the vortex can dramatically alter the shape of the waveform. It appears that in the case of the vortex passing below the airfoil, this passage results in the sonic point moving forward on the bottom surface during the initial passage of the vortex. As was previously mentioned, the movement of this sonic point results in different portions of the disturbance in the leading edge region propagating forward. Thus, the time histories below the airfoil axis show the wave to be delayed beyond that due to the vortex colliding head-on or above the airfoil. Examining the Transonic Small Disturbance boundary condition one sees that this is due to the effect of the u-velocity component. Correctly incorporating this effect seems to be important for accurately predicting the sonic point and the subsequent acoustic propagation.

10. Summary And Conclusions

In this paper a comparison was made between numerical solutions to the Linearized Transonic Small Disturbance Equation, Transonic Small Disturbance Equation, the Euler Equations, and the Navier-Stokes Equations. Although the LTSD and TSD methods were able to properly propagate acoustic waves, they were unable to accurately capture the initial formation of the acoustic waves. This appears to be due to the inaccuracies introduced in the leading edge region, where the initial formation takes place. The fifth-order, upwind-biased scheme used to calculate the solutions to the Euler and Navier-Stokes Equations is well suited to investigating the acoustics due to the fact that the high order accuracy and low dissipation accurately capture and propagate the acoustic wave. The Euler Equations give the same results as the Navier-Stokes Equations for the results presented, and is therefore the best code to use for extensive comparisons of acoustic propagations. It is unknown at this time whether a Full Potential code would be adequate.

The three subcritical cases studied indicate that when non-linear terms are negligible it does not matter whether the vortex passes above or below the airfoil, in either case the amplitude of the waves will be of comparable magnitude. However, the amplitude of the waves will increase as the miss-distance is decreased.

The three supercritical cases indicate that non-linear contributions to the airfoil-vortex interaction are properly captured through wave steepening. The resulting solution is much more complicated due to the formation of supersonic pockets. This requires the accurate calculation of the leading edge region in order to properly calculate the beginning of this supersonic region. The amplitude of the acoustic wave below the airfoil is significantly greater when the vortex passes above the airfoil as compared to it passing below the airfoil. In fact, it is as large as the case of a head-on collision. Therefore, situations which cause the vortex to pass above the airfoil should be avoided when the flow is supercritical.

11. References

1. George, A. R., and Chang, S. B., "Noise due to Transonic Blade-Vortex Interactions," Paper A-83-39-50-D000, 39th Annual National Forum of the American Helicopter Society, St. Louis, Missouri, May 1983.
2. Wu, J. C., Sankar, N. L., and Hsu, T. M., "Unsteady Aerodynamics of an Airfoil Encountering a Passing Vortex," AIAA Paper 85-0203, Reno, Nevada, 1985.
3. Srinivasan, G. R., and McCroskey, W. J., "Numerical Simulations of Unsteady Airfoil-Vortex Interactions," Vertica, Vol. 11, No. 1/2, 1987, pp.3-28.
4. Jones, H. E., and Caradonna, F. X., "Full-Potential Modeling of Blade-Vortex Interactions," Paper No. 27, 12th European Rotorcraft Forum, Garmish-Partenkirchen, Germany, 1986.
5. Rai, M. M., "Navier-Stokes Simulation of Blade-Vortex Interaction Using High-Order Accurate Upwind Schemes," AIAA Paper 87-0543, Reno, Nevada, 1987.
6. Hardin, J. C., Mason, J. P., "A New Look at Sound Generation by Blade/Vortex Interaction," Paper No. 2, Winter Annual Meeting of the ASME, New Orleans, Louisiana, 1984.
7. Lyrintzis, A. S., and George, A. R., "Transonic Blade-Vortex Interactions: The Far Field," AHS National Specialists' Meeting on Aerodynamics and Aeroacoustics, Arlington, Texas, February 1987.
8. Baeder, J. D., McCroskey, W. J., and Srinivasan, G. R., "Acoustic Propagation Using Computational Fluid Dynamics," 42nd Annual Forum of the American Helicopter Society, Washington, D.C., June 1986.
9. Ballhaus, W. F., and Goorjian, P. M., "Implicit Finite-Difference Computations of Unsteady Transonic Flows about Airfoils," AIAA Journal, Vol. 15, No. 12, Dec. 1977, pp. 1728-1735.
10. McCroskey, W. J., and Goorjian, P. M., "Interactions of Airfoils with Gusts and Concentrated Vortices in Unsteady Transonic Flow," AIAA Paper 83-1691, Danvers, Massachusettes, 1983.

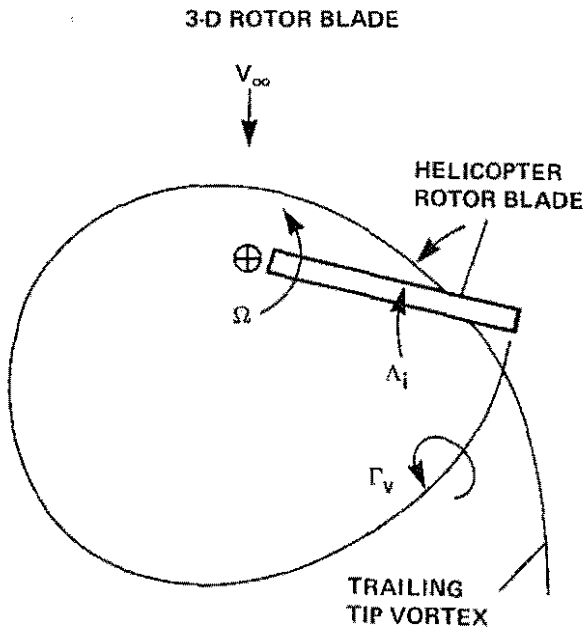

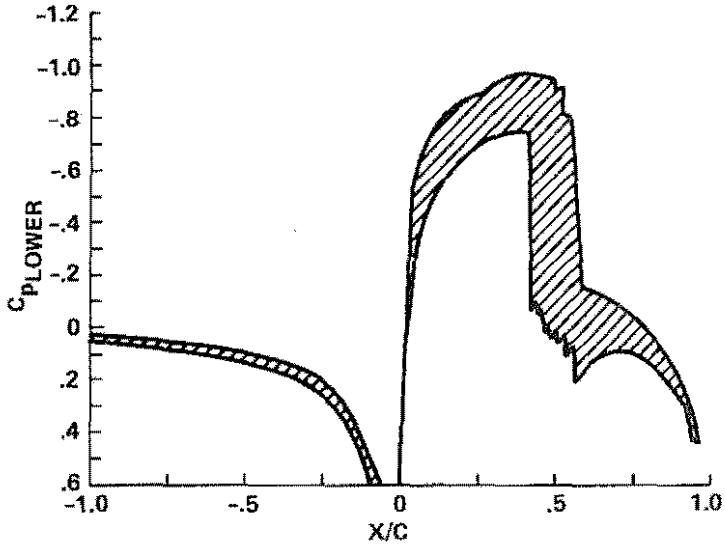

Figure 2. Fluctuating Pressure Along Axis - NACA0012 Airfoil, $M_\infty = .80$, $y_v = -0.26, \Gamma_v = 0.20$

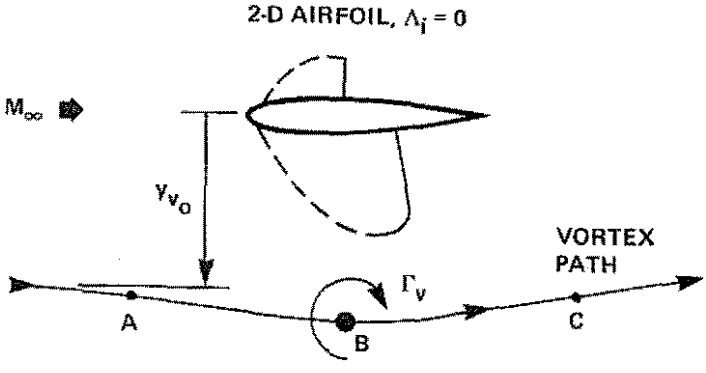

Figure 1. Unsteady Vortex Interactions

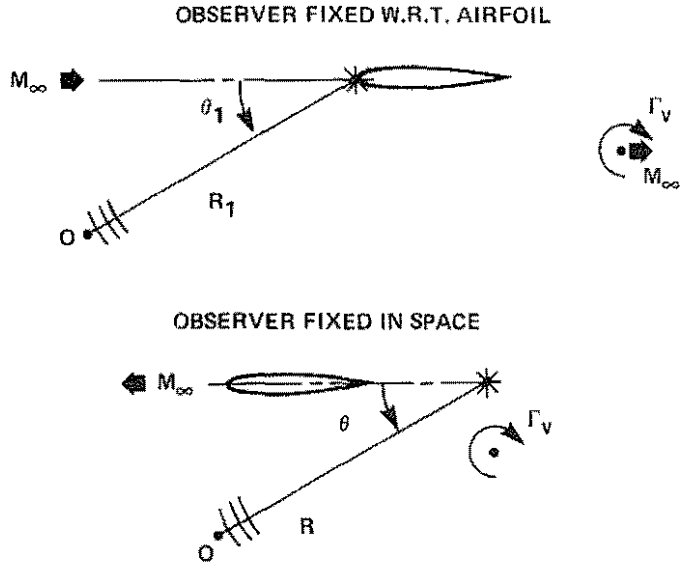

Figure 3. Frames of Reference

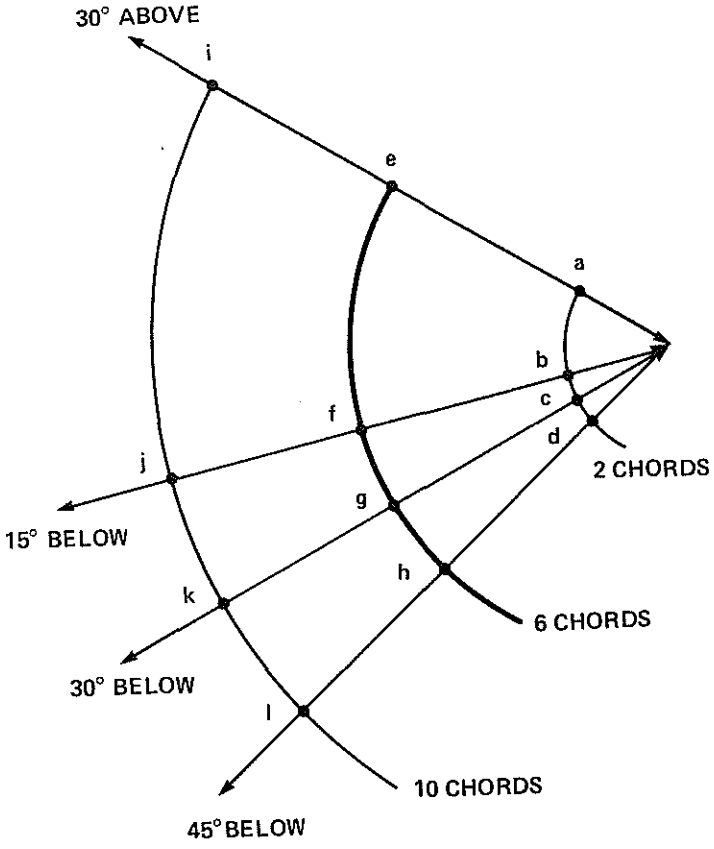

Figure 4. Location of Time Histories to be Presented (In Acoustic Frame)

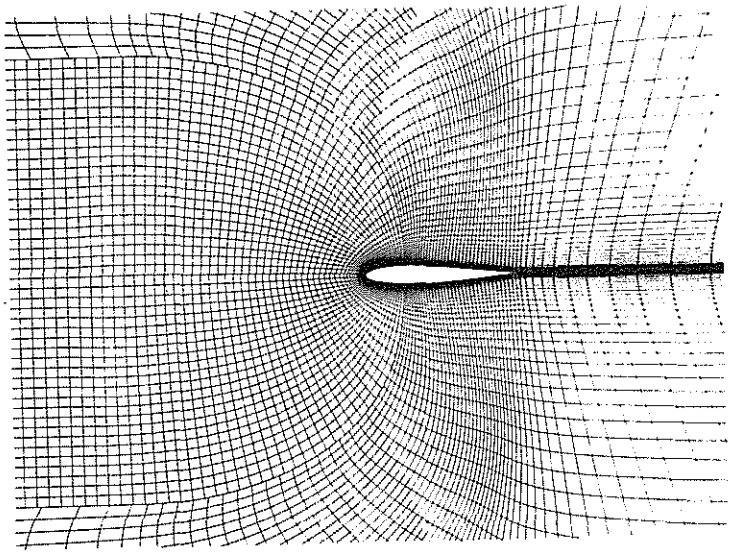

a) Close-up View

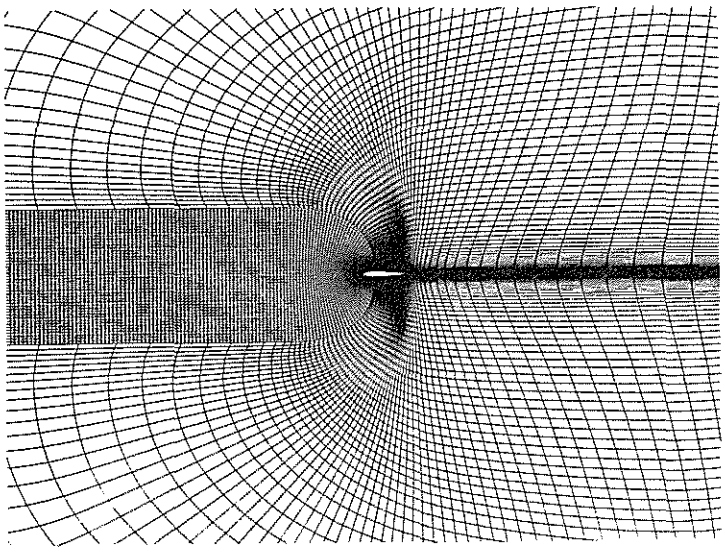

b) Far-field View

Figure 5. Computational Grid (Every Second Line Shown)

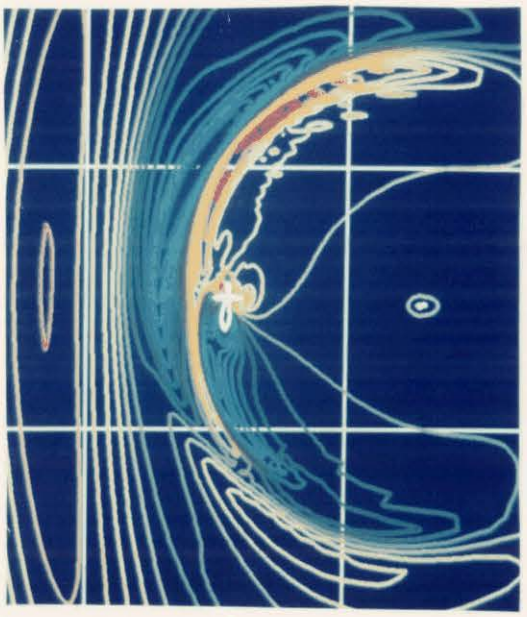

a) Transonic Small Disturbance

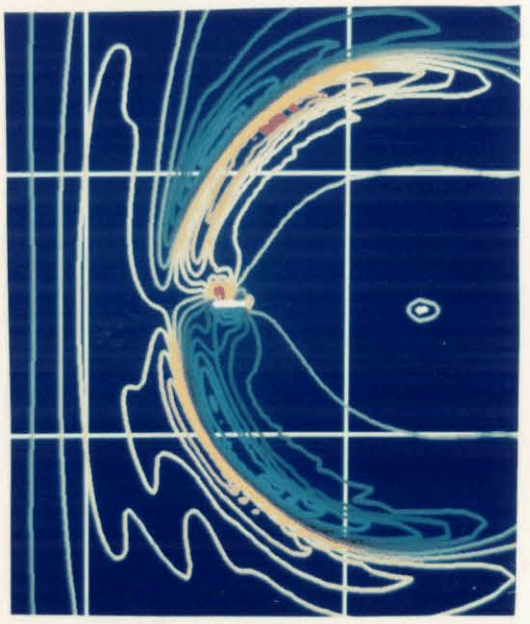

b) Linearized Transonic Small Disturbance

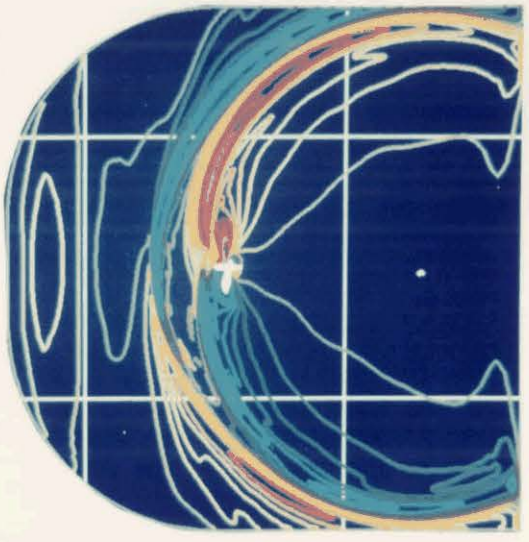

c) Euler

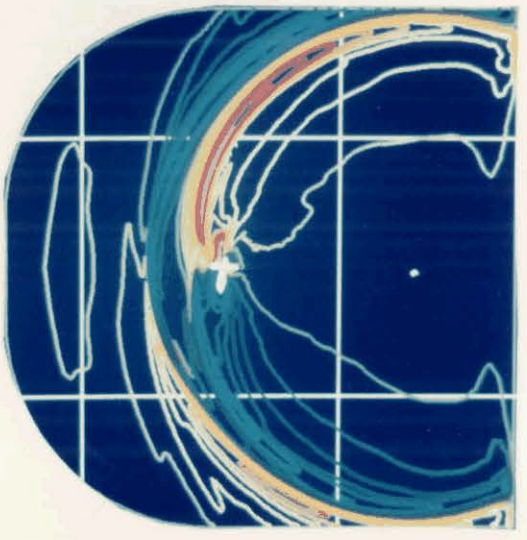

d) Navier-Stokes

Figure 6. Contour Plots for Four Methodologies -
Scaled Pressure Disturbances - $(C_p - C_{p_i}) * Sqrt(R)$ at $x_v = 8.00$
NACA0012 Airfoil, $M_\infty = .80, y_v = -0.26, \Gamma_v = 0.20$

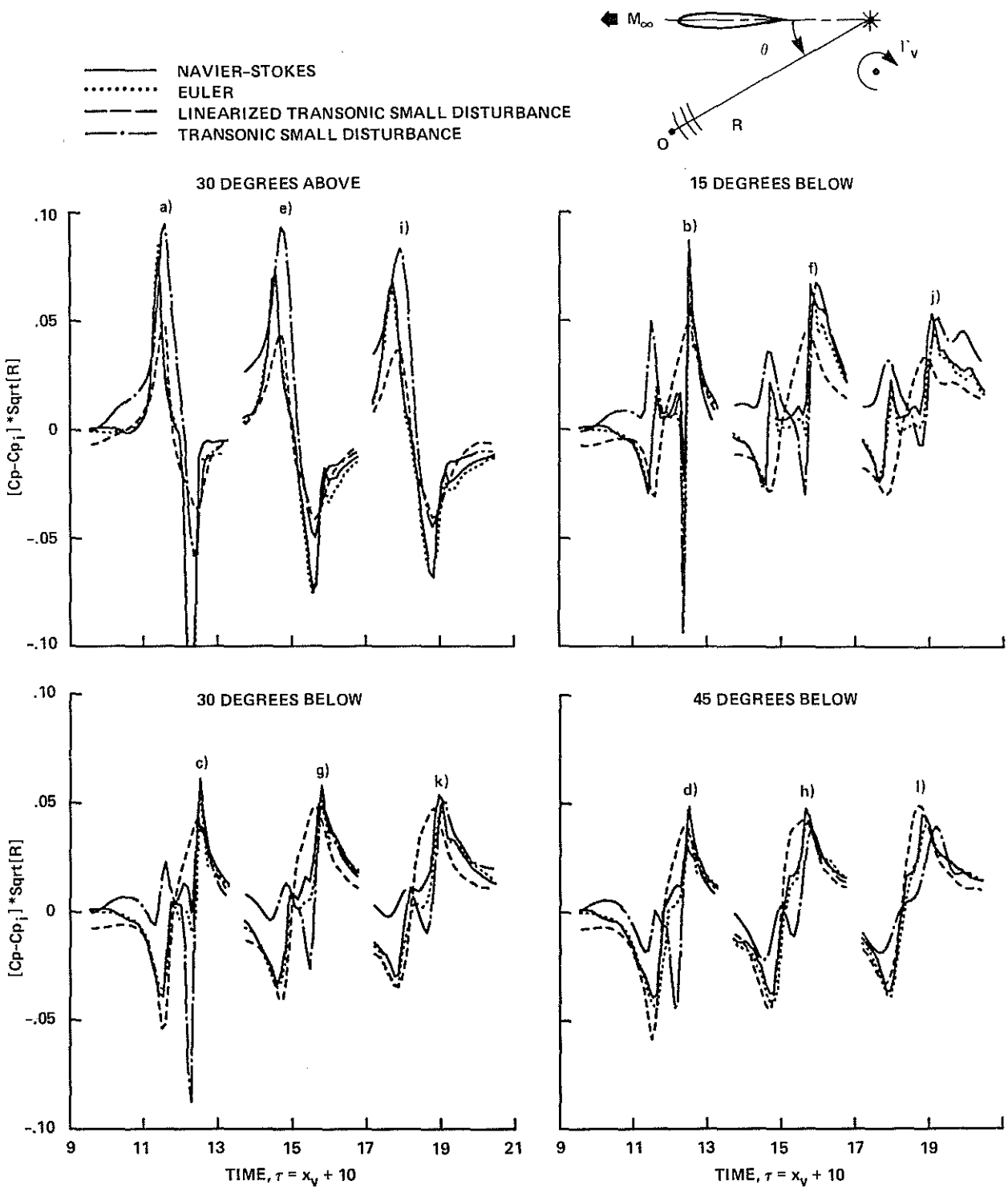

Figure 7. Time Histories for Four Methodologies -
Scaled Pressure Disturbance - $(C_p - C_{p_i}) * Sqrt(R)$
NACA0012 Airfoil, $M_\infty = .80, y_v = -0.26, \Gamma_y = 0.20$

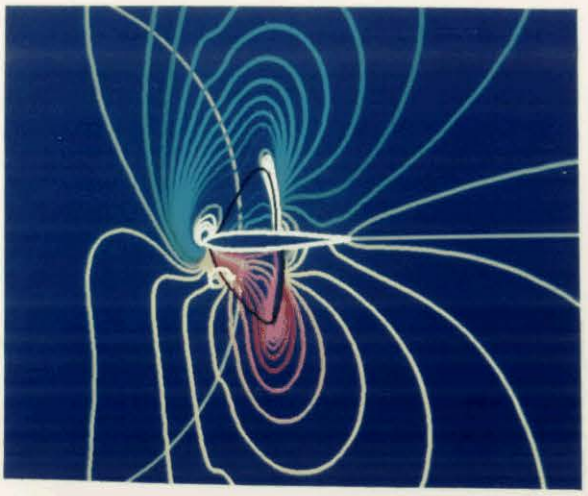

a) $x_v = 0.1$

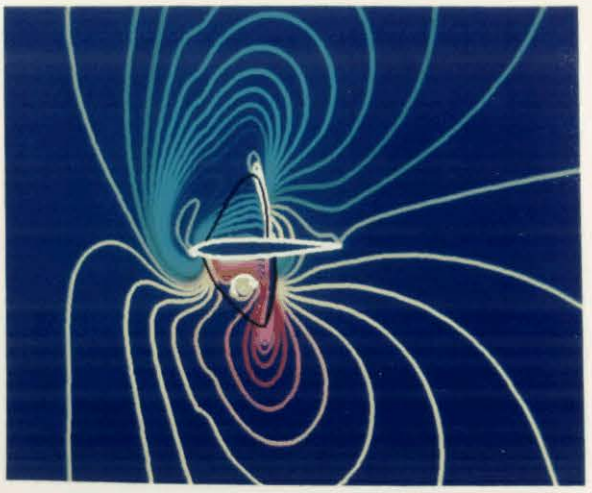

b) $x_v = 0.4$

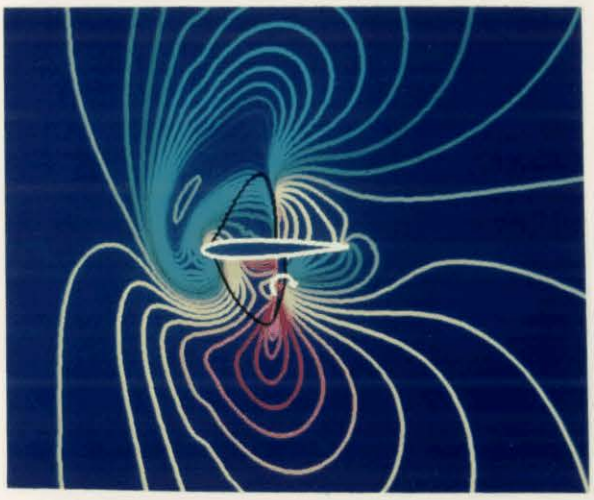

c) $x_v = 0.6$

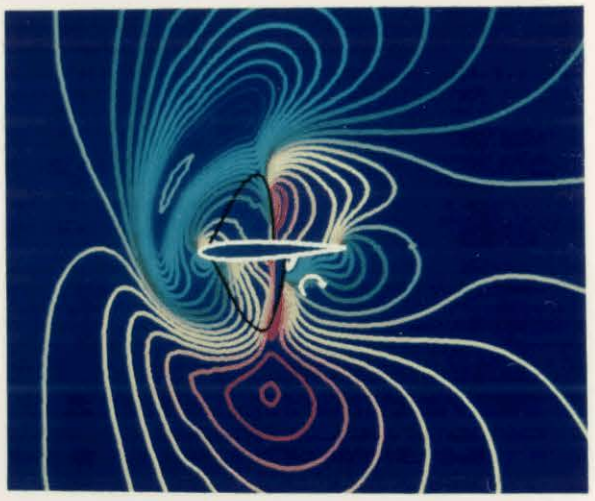

d) $x_v = 0.8$

e) $x_v = 1.0$

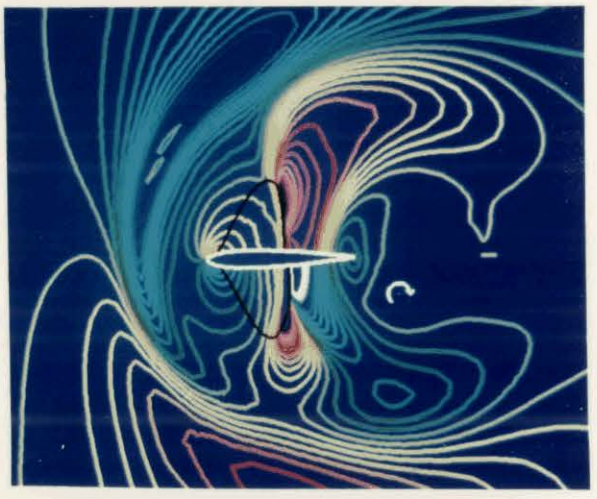

f) $x_v = 1.2$

Figure 8. Contour Plots for Euler Solution -
Scaled Pressure Disturbance - $(C_p - C_{p_i}) * Sqrt(R)$
NACA0012 Airfoil, $M_\infty = .80, y_v = -0.26, \Gamma_y = 0.20$

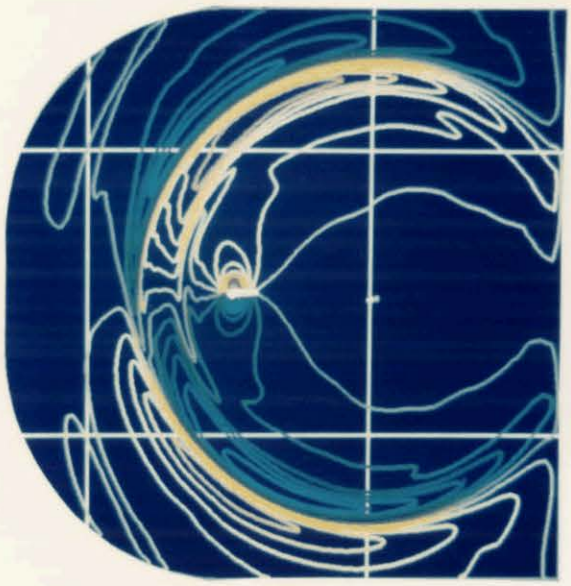

a) Vortex Path Below Airfoil ($y_v = -0.26$)

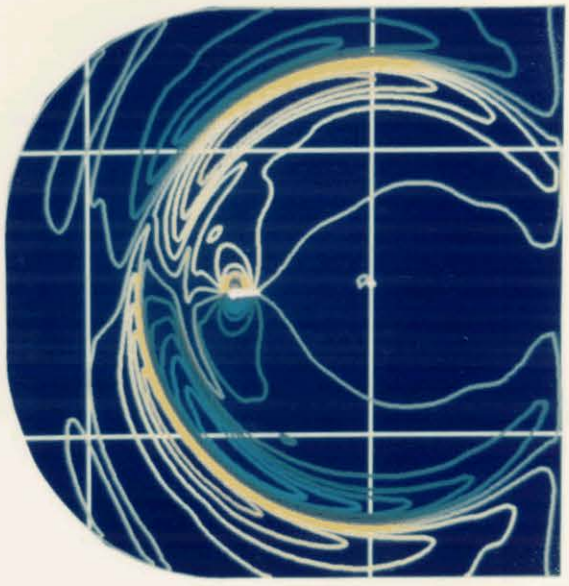

b) Vortex Path Above Airfoil ($y_v = 0.26$)

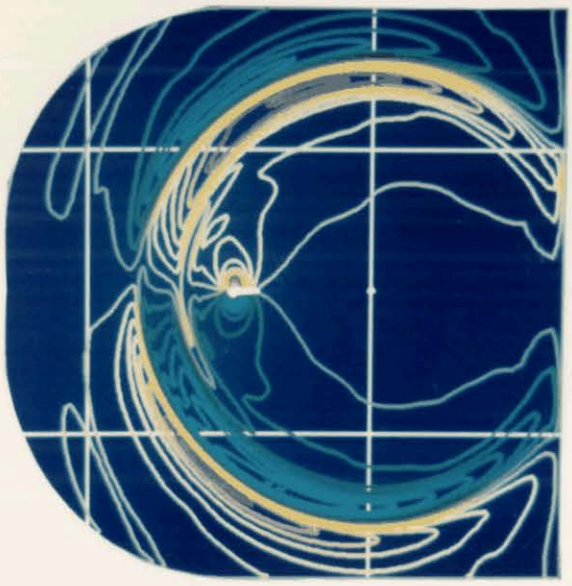

c) Head-on Collision with Airfoil ($y_v = 0.00$)

Figure 9. Contour Plots for Subcritical Cases -
Scaled Pressure Disturbance - $(C_p - C_{p_i}) * Sqrt(R)$ at $x_v = 5.00$
NACA0012 Airfoil, $M_\infty = .60, \Gamma_y = 0.20$

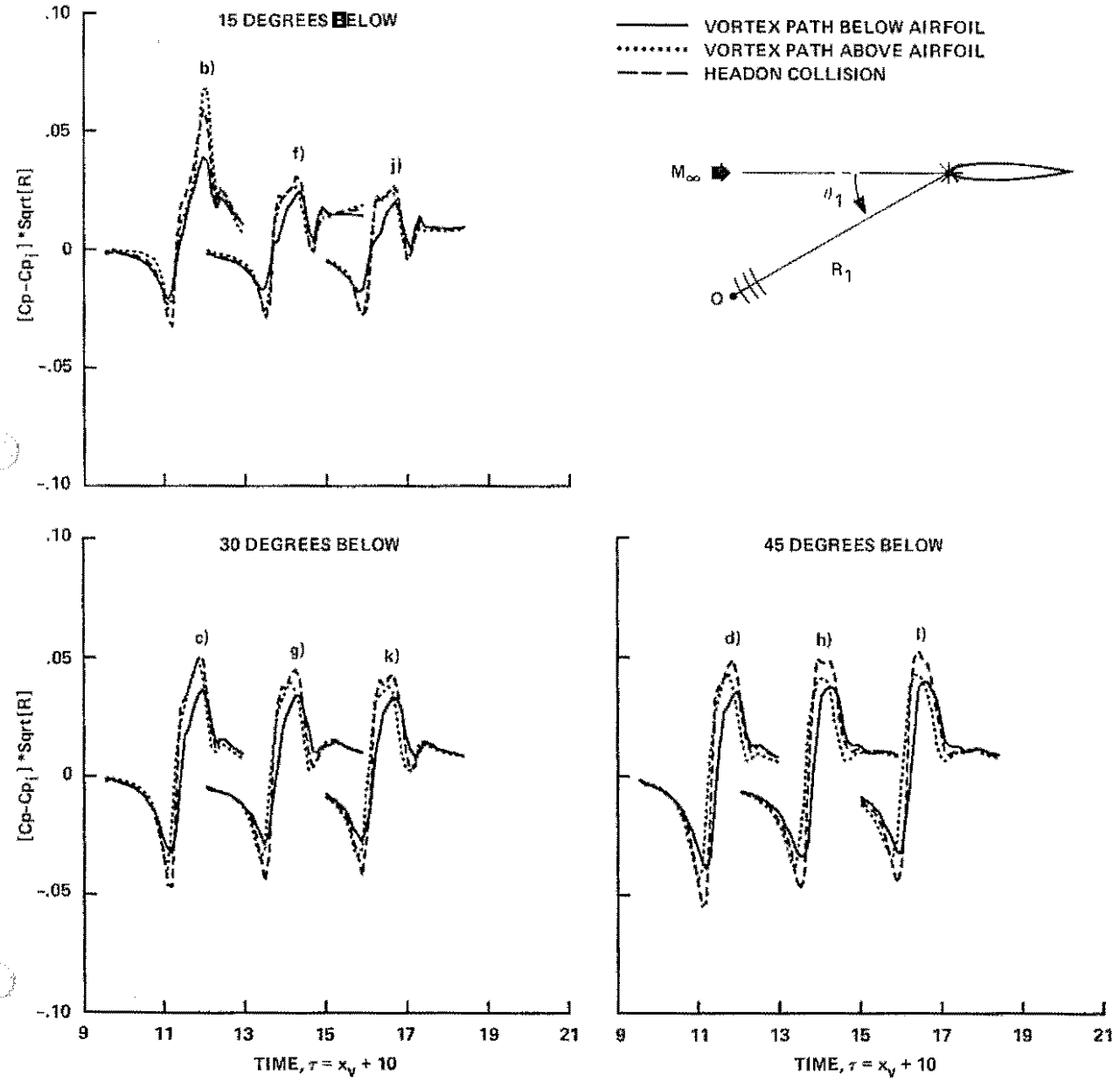

Figure 10. Time Histories for Subcritical Cases -
Scaled Pressure Disturbance - $(C_p - C_{p_i}) * Sqrt(R)$
NACA0012 Airfoil, $M_\infty = .60, \Gamma_y = 0.20$

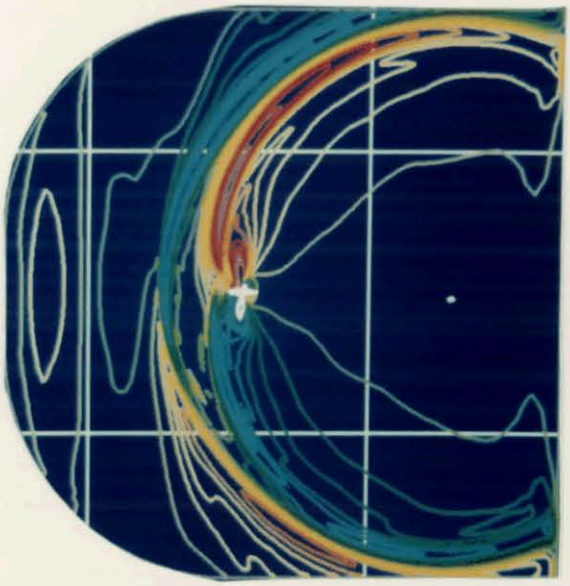

a) Vortex Path Below Airfoil ($y_v = -0.26$)

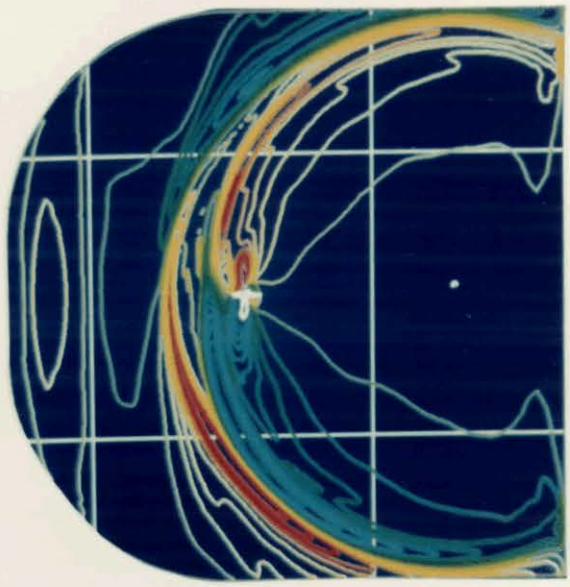

b) Vortex Path Above Airfoil ($y_v = 0.26$)

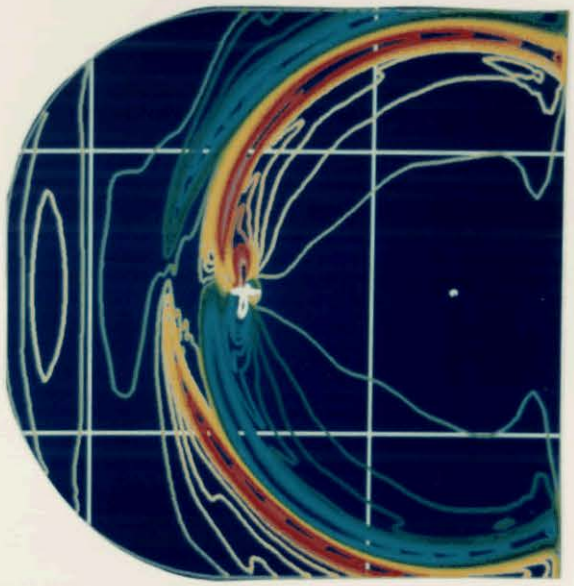

c) Head-on Collision with Airfoil ($y_v = 0.00$)

Figure 11. Contour Plots for Supercritical Cases -
Scaled Pressure Disturbance - $(C_p - C_{p_i}) * Sqrt(R)$ at $x_v = 8.00$
NACA0012 Airfoil, $M_\infty = .80, \Gamma_y = 0.20$

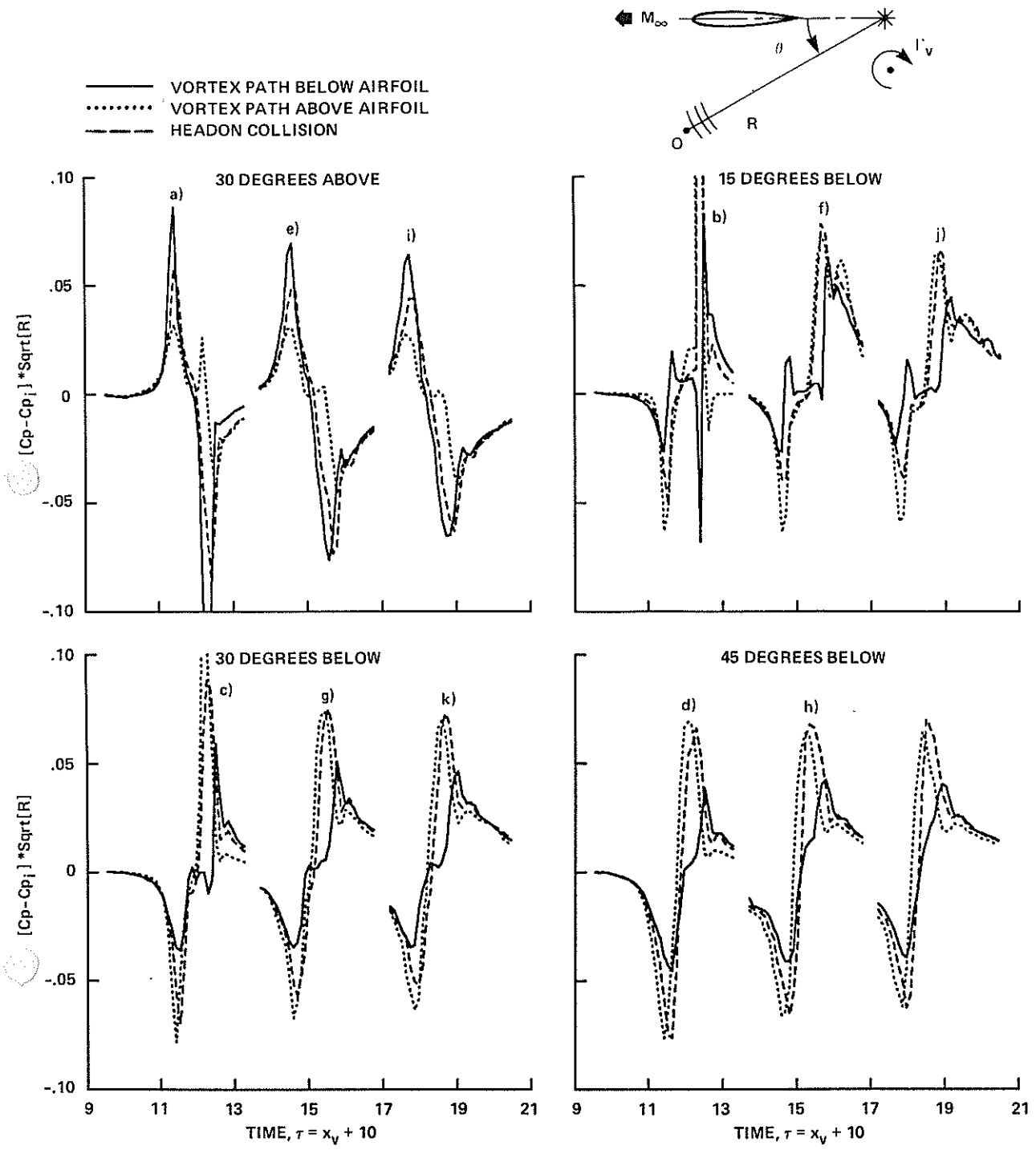

Figure 12. Time Histories for Supercritical Cases -
Scaled Pressure Disturbance - $(C_p - C_{p_i}) * Sqrt(R)$
NACA0012 Airfoil, $M_\infty = .80, \Gamma_y = 0.20$